


## Nematic spectral signatures of the Hund's metal

Laura Fanfarillo <sup>1,2</sup>, Angelo Valli <sup>3</sup>, and Massimo Capone <sup>1</sup>

<sup>1</sup>*Scuola Internazionale Superiore di Studi Avanzati (SISSA), Via Bonomea 265, 34136 Trieste, Italy*

<sup>2</sup>*Department of Physics, University of Florida, Gainesville, Florida 32611, USA*

<sup>3</sup>*Institute for Theoretical Physics, Vienna University of Technology, 1040 Vienna, Austria*

 (Received 6 April 2022; revised 20 December 2022; accepted 14 February 2023; published 27 February 2023)

We show, by means of dynamical mean-field theory calculations, that the experimental fingerprints of the nematic order in iron-based superconductors are intrinsically connected with the electronic correlations in the Hund's correlated metallic state and they cannot be accessed via a renormalized quasiparticle picture. In particular, our results show that (i) in a metal in which correlations are dominated by the Hund's coupling the nematic ordering does not produce a rigid energy shift in the photoemission spectra, but a much richer spectral weight redistribution which mirrors the experimental results, and (ii) the nematic ordering is characterized by an orbital-selective coherence induced by the Hund's physics in agreement with the experimental picture.

DOI: [10.1103/PhysRevB.107.L081114](https://doi.org/10.1103/PhysRevB.107.L081114)

Several quantum materials display a large anisotropy in the electronic properties which has been identified as a signature of electronic nematic order where the in-plane rotational symmetry of the electron fluid is broken making  $x$  and  $y$  directions inequivalent. This appears to be an ubiquitous phenomenon in iron-based superconductors (FeSCs) [1–4].

Among the different experimental probes, a crucial piece of information can be obtained by angle-resolved photoemission spectroscopy (ARPES) exploiting different polarizations of light to selectively probe different iron orbitals. This is particularly relevant in light of the prominent role of the orbital degree of freedom in the electronic structure of FeSC [5]. ARPES studies reveal that the band dispersion in the nematic phase is characterized by a momentum-modulated energy splitting of the  $xz$  and  $yz$  orbitals. Early studies mainly focused on FeSe [6–9] where nematicity emerges in the absence of long-range magnetic order, but the same pattern has been later observed in  $\text{BaFe}_2\text{As}_2$  [10]. Only recently in-depth investigations revealed that the nematic order does not only affect the band dispersion, but also the incoherent spectral weight redistribution [11–13]. Interestingly, the  $xz/yz$  orbital differentiation appears at high frequencies with an opposite sign with respect to the orbital splitting of the bands at the Fermi energy.

A large body of experimental evidence suggests that the origin of the nematic phase is an electronic instability inducing anisotropy in the  $B_{2g}$  channel [2,3]. Both Ising spin-nematic models and orbital-fluctuation-based approaches have been proposed and extensively discussed in the literature [1,4]. Regardless of the origin of the nematic instability, the characterization of the nematic phase of FeSC as emerging from experiments clearly calls for a theoretical scheme which includes the sizable electron-electron interactions and the consequent correlation effects, which are responsible for the nontrivial redistribution of spectral weight at different energy scales, as well as the presence of orbital-selective coherence

in the many-body nematic state. The crucial role of electron-electron interactions does not come as a surprise after several investigations demonstrating that peculiar, orbital-selective, correlation effects dominate the normal state of the FeSC [14].

The identification of orbital-selective Mott physics is one of the outcomes of a theoretical path which has clarified the central role of the Hund's coupling in the multiorbital systems [14–25]. In this framework, the normal phase has been identified as a Hund's metal, a strongly correlated bad metallic state with distinctive correlation properties [14,15,26–41] that interpolate between a description of incoherent and localized atomic states at high energy and one of coherent states at low energy [4,24,42–45] and in which orbital-selective physics emerges as a consequence of an effective decoupling between orbitals in a high-spin state [14,36,40,46].

While we have a fairly good understanding of the role of electronic correlations in the normal state, much less is known about broken-symmetry phases. The link with the nematic phase has been touched upon in Refs. [47,48] using slave-spin mean-field theories which describe the low-energy excitations as Fermi-liquid quasiparticles. The analysis of the nematic susceptibility in the correlated regime reveals that, if the symmetry between  $xz$  and  $yz$  orbitals is explicitly broken, the nematic order is strongly affected by Hund's driven correlations that stabilize configurations with a small occupation imbalance between the  $xz/yz$  orbitals [47] such as, e.g., the sign-change nematic order experimentally observed in FeSC [6–10].

While these slave-particle studies [47,48] provide a reliable description of the nematic reconstruction of the band dispersion, they cannot access other fundamental properties of the electronic state, such as the spectral weight transfer, which can involve different energy scales, and the coherence of the electronic states with different orbital character. Moreover, a trivial extension of the low-energy results provided by those studies to higher energies would produce a picture completely

opposite to what was recently found by ARPES experiments that revealed an opposite trend in the orbital differentiation observed close to the Fermi energy with respect to what was realized at higher frequencies.

This calls for an analysis of the interplay between electronic correlations and nematic order beyond the Fermi-liquid picture exploited by slave-particles studies. In this Letter we address this issue by analyzing the nematic spectral signatures of the Hund's metal using a theoretical description that contains the dynamical correlations of the Hund's metal as treated within dynamical mean-field theory (DMFT) [49].

Our main result is that the nematic spectral weight transfer in the Hund's metal presents a specific feature that differentiates its phenomenology from the nematicity realized in an ordinary correlated metal characterized by a similar effective mass and density of states at the Fermi level. In an ordinary correlated metal the nematic order produces a rigid symmetric shift of the  $xz/yz$  orbital spectral weight around the Fermi energy. On the contrary, the Hund's metal experiences a strong orbital-selective frequency modulation of the spectra as a result of a nematic symmetry breaking. The frequency dependence of the orbital anisotropy appears nonmonotonic and controlled by multiple energy scales, in contrast to what happens in an ordinary correlated metal in which the characteristic energy of the nematic order dynamic is controlled uniquely by the screened Coulomb repulsion  $U$ . A clear differentiation of the correlation effects encoded in the self-energy renormalization at low frequencies and high frequencies is at the origin of the distinctive features of the nematic spectra of the Hund's metal.

Our work identifies a clear signatures of Hund's metal nematicity that explains the main features of the nontrivial ARPES spectra recently observed in Refs. [12,13], thereby proving that the comprehensive experimental picture that emerges combining the observations of a reconstruction of band dispersion and the spectral weight transfer on the nematic phase of FeSC can be fully understood only accounting for the interplay of nematicity and Hund's metal physics.

In order to study the effect of electronic correlations at a reasonable computational cost we consider a minimal model, already used in Ref. [50], which accounts for the main features of the electronic structure of FeSC and for the electron-electron correlations induced by the combined effect of the Hubbard repulsion  $U$  and the Hund's coupling  $J_H$ . The kinetic Hamiltonian is given by a three-orbital tight-binding model adapted from Ref. [51],  $H_0 = \sum_{\mathbf{k}\sigma} \sum_{\mu\nu} T^{\mu\nu}(\mathbf{k}) c_{\mathbf{k}\mu\sigma}^\dagger c_{\mathbf{k}\nu\sigma}$ , where  $\mu, \nu$  are orbital indices for the  $yz, xz, xy$  orbitals.  $c_{\mathbf{k}\mu\sigma}^\dagger$  ( $c_{\mathbf{k}\mu\sigma}$ ) is the fermionic operators that create (annihilates) an electron in orbital  $\mu$ , with momentum  $\mathbf{k}$  and spin  $\sigma$ . The set of parameters chosen results in a bare bandwidth  $W = 1.6$  eV and reproduces qualitatively the shape and the orbital content of the Fermi surfaces typical of the FeSC family, namely two holelike pockets composed of  $yz$ - $xz$  orbitals at the  $\Gamma$  point and two elliptical electronlike pockets formed by  $xy$  and  $yz/xz$  orbitals centered at the  $X/Y$  point of the 1Fe-Brillouin zone [52]. Local electronic interactions are included considering the multiorbital Kanamori Hamiltonian which parametrizes the electron-electron interactions in terms of a Hubbard-like repulsion  $U$  and an exchange coupling  $J_H$  favoring high-spin states [26].

TABLE I. Quasiparticle renormalization factors extracted by orbital-dependent DMFT self-energy. Starting from degenerate values of  $Z_{xz/yz}$  in the tetragonal phase, orbital differentiation develops in the nematic state with the  $xz$  orbital remaining more coherent than the  $yz$ .

	Tetragonal	Nematic
$J_H = 0.05U$	$Z_{xz/yz} = 0.38$	$Z_{xz} = 0.45, Z_{yz} = 0.18$
$J_H = 0.25U$	$Z_{xz/yz} = 0.25$	$Z_{xz} = 0.35, Z_{yz} = 0.18$

We account phenomenologically for the nematic order by adding to the Hamiltonian a bare nematic perturbation  $\sim \eta(n_{yz} - n_{xz})$ ,  $\eta > 0$ . Rather than looking for a spontaneous nematic symmetry breaking in our simplified model, or considering a specific low-energy origin for the same instability, we focus on the role of the electronic correlations and in particular on their effect on the spectral properties in the nematic phase.

We compute the nematic orbital spectral functions using the full orbital and frequency-dependent DMFT self-energy  $\Sigma_{\mu\mu}(i\omega_n)$ , where  $\omega_n$  is the  $n$ th fermionic Matsubara frequency. The orbital dependence of the self-energy leads to a self-consistent renormalization of the nematic splitting. The effect of correlations within a Fermi-liquid quasiparticle picture, encoded in the quasiparticle weight  $Z_\mu$ , can be extracted from the DMFT self-energy behavior at low frequency as  $Z_\mu = (1 - \partial \text{Im} \Sigma_{\mu\mu} / \partial \omega_n)^{-1}$ . We use an exact diagonalization solver at zero temperature [52–55] at a density of four electrons in three orbitals per site, that reproduces the low-energy electronic structure with hole and electron pockets including the momentum dependence of the nematic splitting [47].

One of our main goals is to assess the effects of dynamical correlations induced by the Hund's coupling on the spectral properties in the nematic phase. In order to highlight these effects, we focus on two correlated regimes having similar values of  $Z_\mu \sim 0.3$  in the tetragonal phase (see Table I), but characterized by different values of the Hund's coupling:  $J_H = 0.05U$ ,  $U \sim W$  define an ordinary correlated metal, while for  $J_H = 0.25U$ ,  $U \sim W$  we are inside the Hund's metal regime. The spectra in the tetragonal state for both cases are shown in Figs. 1(a) and 1(e). In order to directly compare the outcome of our calculations with ARPES experiments [12,13], we plot the spectral function  $A_\mu(\mathbf{k}, \omega)$  integrated between the high-symmetry points  $\Gamma$ - $X/Y$  of the 1Fe-Brillouin zone, for the  $yz/xz$  orbital.

For small  $J_H/U$  we recover the familiar Mott-like behavior where Hubbard bands develop on an energy scale which approaches  $U$  in the strong-coupling limit. For larger  $J_H/U$  we find that the spectral weight reshuffling involves also a significantly smaller energy scale  $\simeq U - 3J_H$ , which emerges as the effective charge-charge repulsion in the Kanamori model [39].

In what follows we analyze the nematic spectra and show that the Hund's metal state is affected by the nematic ordering in a much more subtle way with respect to the low- $J_H/U$  regime. To some extent, the main difference with respect to an ordinary correlated metal is that the low-energy scale

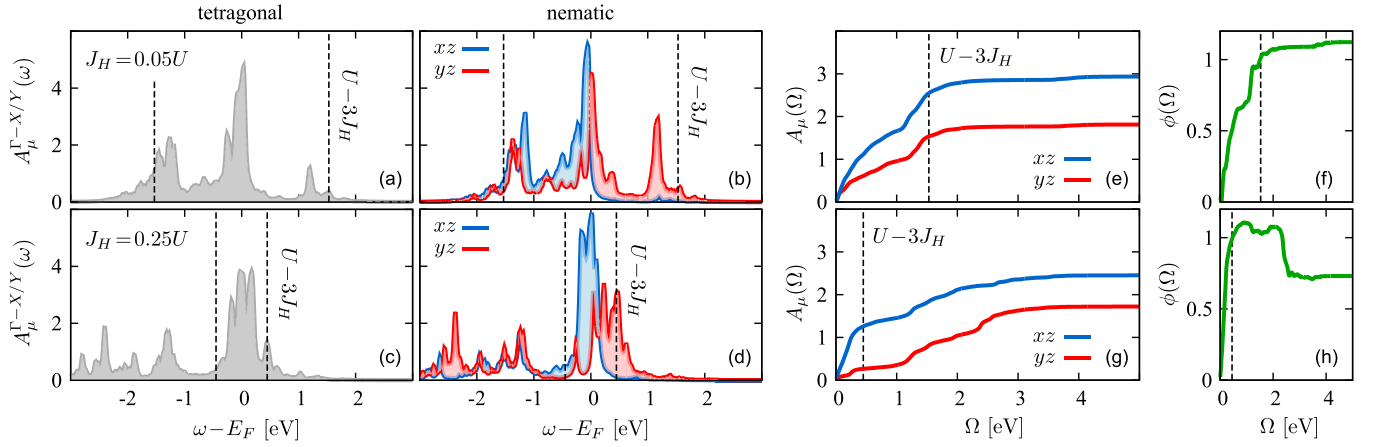


FIG. 1. Spectral function analysis. Orbital spectral function computed using orbital and frequency-dependent DMFT self-energy for  $U \sim W$  (a), (b) in an ordinary correlated metal,  $J_H = 0.05U$  and (c), (d) in a Hund's metal,  $J_H = 0.25U$ . In (a), (c) we report the spectra computed in the tetragonal phase, using  $\delta\epsilon = 0$  and in (b), (d) the ones for the nematic phase, using  $\delta\epsilon = 50$  meV. The nematic order introduces  $xz/yz$  orbital differentiation both in the low- and high- $J_H$  regimes, however, in the ordinary correlated metal (b) this appears as rigid shift of the  $xz/yz$  orbital slightly below/above the Fermi energy, while in the Hund's metal (d) we find an orbital-selective modulation in frequency with the  $xz$  orbital remaining closer to  $E_F$  and the  $yz$  weight moving at higher energy. (e), (g) Frequency integration of the orbital nematic spectra  $A_\mu$  shown in (b), (d) as a function of the cutoff  $\Omega$ . (f), (h) Frequency dependence of the nematic parameter  $\phi = A_{xz} - A_{yz}$ .  $\phi$  grows monotonically up to energy  $\Omega \sim U$  in the low- $J_H$  regime. In the Hund's metal instead it grows rapidly at low frequency reaching its maximum at  $\Omega \sim U - J_H$ , and it is then suppressed and saturates to a constant value at high frequency. The dashed vertical lines in each panel denote the energy scale  $U - 3J_H$ .

where the quasiparticles live is not decoupled from the high-energy ( $\sim U$ ) features that evolve into the Hubbard bands. In the Hund's metal the spectral weight redistribution due to local interactions accumulates also in a narrower energy window around the Fermi energy [16,17,22,38,50]. This feature emerged already as crucial to boost boson-mediated superconductivity in Hund's metal [50] and it is expected to critically affect the interplay between local electronic interactions and other low-energy instabilities including the nematic order.

In Figs. 1(b) and 1(d) we show the nematic orbital spectra for our two choices of parameters:  $J_H = 0.05U$  (ordinary correlated metal) and  $J_H = 0.25U$  (Hund's metal). In both regimes, the nematic order does not alter the overall energy window in which the spectral weight is distributed with respect to the tetragonal phase, however, it produces a differentiation in the  $xz/yz$  orbital coherence. Interestingly, while the differentiation produced in the quasiparticle renormalization factors  $Z_\mu$ , listed in Table I, is similar in the two correlated regimes, the orbital-dependent spectral weight redistribution appears quite different. By comparing the spectra of the ordinary correlated metal in the tetragonal and nematic phase [Figs. 1(a) and 1(b)], we find the  $xz/yz$  orbital weights are rigidly and symmetrically shifted around the Fermi energy  $E_F$ . In the Hund's metal instead [Figs. 1(c) and 1(d)], the orbital weight redistribution is not symmetric and thus the orbital anisotropy of the spectra is much more pronounced. The  $xz$  spectral weight remains closer to  $E_F$  than the  $yz$  [see the larger  $xz$  peak close to  $E_F$  in Fig. 1(d)]. The  $yz$  orbital weight is transferred instead to much higher energies where the Hubbard bands are located. It is worth noticing that this result is due to the dynamic properties of the Hund's metal and cannot be inferred by the analysis of the quasiparticle renormalization factors  $Z_{xz/yz}$ . Those can only account for a rigid shift of the  $xz/yz$  orbital spectral weight

around  $E_F$ , while they cannot reproduce the orbital-selective behavior at higher frequencies observed in the Hund's metal regime.

To better visualize the frequency dependence of the orbital anisotropy of the spectral weight shown in Figs. 1(b) and 1(d), we perform a frequency integration over the occupied states of the spectral function on a window of amplitude  $\Omega$ ,

$$A_{yz/xz}^{\Gamma-X/Y}(\Omega) = \int_{-\Omega}^{\Omega} d\omega \int_{\Gamma}^{X/Y} d\mathbf{k} A_{yz/xz}(\mathbf{k}, \omega), \quad (1)$$

and analyze the dynamics of the nematic spectra parameter  $\phi(\Omega) = A_{xz}(\Omega) - A_{yz}(\Omega)$ . In Figs. 1(e) and 1(f) and Figs. 1(g) and 1(h) we show respectively  $A_{xz/yz}(\Omega)$  and  $\phi(\Omega)$  for the low- and high- $J_H/U$  regimes. In the ordinary correlated metal the anisotropy of the  $A_{xz/yz}$  spectral functions [Fig. 1(e)] and, as a consequence, the nematic parameter  $\phi$  [Fig. 1(f)] grow monotonically at an essentially constant rate as we increase the integration window  $\Omega$  until it reaches values of order  $U$ . On the other hand, in the Hund's metal the orbital spectral functions  $A_{xz/yz}$  [Fig. 1(g)] rapidly deviate from each other for small values of  $\Omega$ , but they even get closer at higher energy due to the orbital frequency modulation visible in Fig. 1(d). As a consequence, the energy dependence of  $\phi$ , shown in Fig. 1(h), is characterized by a fast growth at low energy, while at frequency  $\Omega > U - 3J_H$  the nematic order decreases as a function of  $\Omega$  and saturates at higher frequencies to a value approximately  $\sim 0.75$  of the maximum.

To clarify the physical origin of the behavior of the nematic spectral weight in the Hund's metal we look at the self-energy on the imaginary Matsubara axis in the two different correlated cases, which allows us to disentangle the interaction-driven contribution to the single-particle spectra shown in Figs. 1(b) and 1(d). In Fig. 2 we show the imaginary and real parts of the self-energy in the two correlated

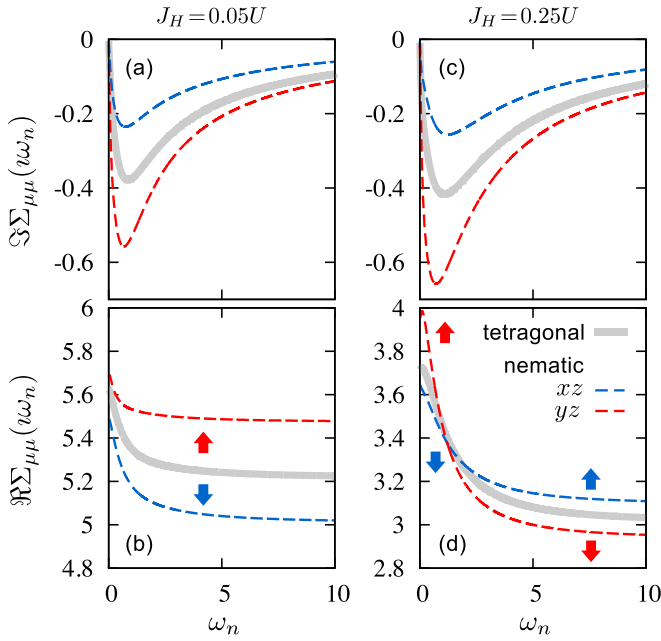


FIG. 2. Matsubara orbital-resolved self-energy in the tetragonal (solid gray lines) and nematic phase (color dashed lines) for (a), (b)  $J_H = 0.05U$  and (c), (d)  $J_H = 0.25U$ . The slope of the imaginary part yields the anisotropy of the orbital coherence  $Z_{xz} > Z_{yz}$  and shows the same qualitative behavior regardless of the value of  $J_H$ . Instead  $\text{Re } \Delta\Sigma_{\mu\mu}$ , obtained as the difference between the nematic and tetragonal self-energies for each orbital, is strongly affected by the Hund's coupling. While having always an opposite sign for the  $xz$  and  $yz$  orbitals, at  $J_H = 0.05U$  it has the same sign as the nematic perturbation and is weakly frequency dependent (i.e., it results in a nearly rigid shift), while at  $J_H = 0.25U$  it changes sign between low and high energies, reflecting the complex spectral weight redistribution in the Hund's metal.

regimes and contrast the nematic results with the tetragonal ones. The imaginary part [Fig. 2(a) and 2(c)], whose low-frequency behavior provides an estimate of the quasiparticle weight  $Z_\mu$ , has the same qualitative behavior in the two cases, showing a finite value of  $Z_\mu$  which becomes larger for the  $xz$  orbital and smaller for the  $yz$  one (see Table I). This effect recovers what was found within the Fermi-liquid quasiparticle approximation by previous investigations via slave-particle methods [47,48]. The real part of the self-energy shows instead a remarkable difference within the two correlated cases. While for small  $J_H/U$ , panel [Fig. 2(b)] the orbital-resolved change of the self-energy follows the nematic perturbation at every frequency, for sizable  $J_H/U$  [Fig. 2(d)] there is a change of sign at some finite frequency, meaning that only the low-energy part of the spectrum follows the sign of the nematic perturbation, while the high-energy spectrum moves in the opposite direction. This is a clearly nontrivial result that cannot be deduced from the analysis of the orbital anisotropy of the quasiparticle weight  $Z_\mu$ , and required instead a proper inclusion of correlations at the DMFT level in order to differentiate

low- and high-frequency behaviors. The frequency modulation characterized by the real part of the self-energy in the Hund's metal regime is at the origin of the remarkably different redistribution of the orbital spectral weight in the low-versus high- $J_H/U$  regimes shown in Figs. 1(b) and 1(d).

By comparing our theoretical findings to the recent ARPES results on the orbital coherence in the nematic phase of FeSC [12,13] we argue that the experimental spectra show clear signatures of Hund's metal nematicity characterized by an orbital-selective spectral weight redistribution qualitatively compatible with Fig. 1(d) and a frequency-modulated nematic order with an intermediate-energy contribution which partially cancels the low-energy signal as shown in Fig. 1(h). The peculiar behavior of the nematic spectra is traced down to a frequency-modulated orbital differentiation of the real part of the self-energy in the Hund's metal that displays opposite sign at low versus high frequencies as shown in Fig. 2(d).

In conclusion, we have analyzed the effects of electronic correlations including the Hund's exchange coupling on the nematic phase of a multiorbital model for iron-based superconductors. Comparing results for small values of the Hund's coupling, which behave as a standard Mott-Hubbard system, with large values of  $J_H$ , that drive the system into a Hund's metal, we are able to demonstrate that the effects of strong correlations on the nematic order cannot be described merely in terms of an orbital-dependent quasiparticle weight reflecting the differentiation between the  $xz$  and  $yz$  orbitals. Rather, the full frequency dependence of the interaction effects must be taken into account.

Our analysis allows us to clearly identify the distinctive signatures of the nematic spectra of a Hund's metal characterized by a frequency dependence of the nematic order originated by an opposite orbital differentiation of the self-energy at low and high frequencies.

Our results are in excellent agreement with experimental ARPES spectra that show how the nematic reconstruction of band dispersion is accompanied by a nontrivial spectral weight transfer. The ability of our results to reproduce the complex experimental picture strongly supports the physical picture where the broken-symmetry phases observed in iron-based superconductors and other Hund's correlated metals can only be understood in terms of instabilities of the Hund's metal and a successful theory of these phenomena should include the dynamical correlation effects characteristic of the Hund's metal.

We are grateful to H. Pfau for helpful discussions. L.F. acknowledges financial support from the European Union Horizon 2020 research and innovation programme under the Marie Skłodowska-Curie grant SuperCoop (Grant No. 838526). A.V. acknowledges financial support from the Austrian Science Fund (FWF) through through project P 31631. M.C. acknowledges financial support from MIUR through the PRIN 2017 (Prot. 20172H2SC4 005) programs and Horizon 2020 through the ERC project FIRSTORM (Grant Agreement No. 692670).

[1] R. M. Fernandes, A. V. Chubukov, and J. Schmalian, *Nat. Phys.* **10**, 97 (2014).

[2] A. E. Bohmer and C. Meingast, *C. R. Phys.* **17**, 90 (2016).

[3] Y. Gallais and I. Paul, *C. R. Phys.* **17**, 113 (2016).



- [4] R. M. Fernandes, A. I. Coldea, H. Ding, I. R. Fisher, P. J. Hirschfeld, and G. Kotliar, *Nature (London)* **601**, 35 (2022).
- [5] M. Yi, Y. Zhang, Z.-X. Shen, and D. Lu, *npj Quantum Mater.* **2**, 57 (2017).
- [6] Y. Suzuki, T. Shimojima, T. Sonobe, A. Nakamura, M. Sakano, H. Tsuji, J. Omachi, K. Yoshioka, M. Kuwata-Gonokami, T. Watashige *et al.*, *Phys. Rev. B* **92**, 205117 (2015).
- [7] L. Fanfarillo, J. Mansart, P. Toulemonde, H. Cercellier, P. Le Fèvre, F. Bertran, B. Valenzuela, L. Benfatto, and V. Brouet, *Phys. Rev. B* **94**, 155138 (2016).
- [8] Y. Zhang, M. Yi, Z.-K. Liu, W. Li, J. J. Lee, R. G. Moore, M. Hashimoto, M. Nakajima, H. Eisaki, S.-K. Mo *et al.*, *Phys. Rev. B* **94**, 115153 (2016).
- [9] M. Yi, H. Pfau, Y. Zhang, Y. He, H. Wu, T. Chen, Z. R. Ye, M. Hashimoto, R. Yu, Q. Si *et al.*, *Phys. Rev. X* **9**, 041049 (2019).
- [10] H. Pfau, S. D. Chen, M. Yi, M. Hashimoto, C. R. Rotundu, J. C. Palmstrom, T. Chen, P.-C. Dai, J. Straquadine, A. Hristov *et al.*, *Phys. Rev. Lett.* **123**, 066402 (2019).
- [11] C. Cai, T. T. Han, Z. G. Wang, L. Chen, Y. D. Wang, Z. M. Xin, M. W. Ma, Y. Li, and Y. Zhang, *Chin. Phys. B* **29**, 077401 (2020).
- [12] H. Pfau, S. D. Chen, M. Hashimoto, N. Gauthier, C. R. Rotundu, J. C. Palmstrom, I. R. Fisher, S.-K. Mo, Z.-X. Shen, and D. Lu, *Phys. Rev. B* **103**, 165136 (2021).
- [13] H. Pfau, M. Yi, M. Hashimoto, T. Chen, P.-C. Dai, Z.-X. Shen, S.-K. Mo, and D. Lu, *Phys. Rev. B* **104**, L241101 (2021).
- [14] L. de' Medici, G. Giovannetti, and M. Capone, *Phys. Rev. Lett.* **112**, 177001 (2014).
- [15] Z. P. Yin, K. Haule, and G. Kotliar, *Nat. Mater.* **10**, 932 (2011).
- [16] L. de' Medici, *Phys. Rev. B* **83**, 205112 (2011).
- [17] P. Werner, M. Casula, T. Miyake, F. Aryasetiawan, A. J. Millis, and S. Biermann, *Nat. Phys.* **8**, 331 (2012).
- [18] F. Hardy, A. E. Böhmer, D. Aoki, P. Burger, T. Wolf, P. Schweiss, R. Heid, P. Adelman, Y. X. Yao, G. Kotliar *et al.*, *Phys. Rev. Lett.* **111**, 027002 (2013).
- [19] J. Malet, V. B. Zabolotnyy, D. V. Evtushinsky, S. Thirupathaiah, A. U. B. Wolter, L. Harnagea, A. N. Yaresko, A. N. Vasiliev, D. A. Chareev, A. E. Bohmer, F. Hardy, T. Wolf, C. Meingast, E. D. L. Rienks, B. Buchner, and S. V. Borisenko, *Phys. Rev. B* **89**, 220506(R) (2014).
- [20] M. Yi, Z.-K. Liu, Y. Zhang, R. Yu, J.-X. Zhu, J. Lee, F. Moore, R.G. and Schmitt, W. Li, S. Riggs, J.-H. Chu *et al.*, *Nat. Commun.* **6**, 7777 (2015).
- [21] D. E. McNally, S. Zellman, Z. P. Yin, K. W. Post, H. He, K. Hao, G. Kotliar, D. Basov, C. C. Homes, and M. C. Aronson, *Phys. Rev. B* **92**, 115142 (2015).
- [22] S. Backes, H. O. Jeschke, and R. Valentí, *Phys. Rev. B* **92**, 195128 (2015).
- [23] F. Hardy, A. E. Böhmer, L. de' Medici, M. Capone, G. Giovannetti, R. Eder, L. Wang, M. He, T. Wolf, P. Schweiss *et al.*, *Phys. Rev. B* **94**, 205113 (2016).
- [24] S. Lafuerza, H. Gretarsson, F. Hardy, T. Wolf, C. Meingast, G. Giovannetti, M. Capone, A. S. Sefat, Y.-J. Kim, P. Glatzel *et al.*, *Phys. Rev. B* **96**, 045133 (2017).
- [25] M. D. Watson, S. Backes, A. A. Haghighirad, M. Hoesch, T. K. Kim, A. I. Coldea, and R. Valentí, *Phys. Rev. B* **95**, 081106(R) (2017).
- [26] A. Georges, L. de' Medici, and J. Mravlje, *Annu. Rev. Condens. Matter Phys.* **4**, 137 (2013).
- [27] P. Werner, E. Gull, M. Troyer, and A. J. Millis, *Phys. Rev. Lett.* **101**, 166405 (2008).
- [28] K. Haule and G. Kotliar, *New J. Phys.* **11**, 025021 (2009).
- [29] L. de' Medici, S. R. Hassan, M. Capone, and X. Dai, *Phys. Rev. Lett.* **102**, 126401 (2009).
- [30] H. Ishida and A. Liebsch, *Phys. Rev. B* **81**, 054513 (2010).
- [31] A. Liebsch and H. Ishida, *Phys. Rev. B* **82**, 155106 (2010).
- [32] L. de' Medici, J. Mravlje, and A. Georges, *Phys. Rev. Lett.* **107**, 256401 (2011).
- [33] R. Yu and Q. Si, *Phys. Rev. B* **86**, 085104 (2012).
- [34] E. Bascones, B. Valenzuela, and M. J. Calderón, *Phys. Rev. B* **86**, 174508 (2012).
- [35] N. Lanatà, H. U. R. Strand, G. Giovannetti, B. Hellsing, L. de' Medici, and M. Capone, *Phys. Rev. B* **87**, 045122 (2013).
- [36] L. Fanfarillo and E. Bascones, *Phys. Rev. B* **92**, 075136 (2015).
- [37] L. de' Medici, *Weak and Strong Correlations in Fe Superconductors* (Springer, Cham, 2015).
- [38] K. Stadler, G. Kotliar, A. Weichselbaum, and J. von Delft, *Ann. Phys.* **405**, 365 (2019).
- [39] A. Isidori, M. Berović, L. Fanfarillo, L. de' Medici, M. Fabrizio, and M. Capone, *Phys. Rev. Lett.* **122**, 186401 (2019).
- [40] A. Mezio and R. H. McKenzie, *Phys. Rev. B* **100**, 205134 (2019).
- [41] A. Richaud, M. Ferraretto, and M. Capone, *Phys. Rev. B* **103**, 205132 (2021).
- [42] T. Chen, Y. Chen, A. Kreisel, X. Lu, A. Schneidewind, Y. Qiu, J. T. Park, T. G. Perring, J. R. Stewart, H. Cao *et al.*, *Nat. Mater.* **18**, 709 (2019).
- [43] X. Lu, W. Zhang, Y. Tseng, R. Liu, Z. Tao, E. Paris, P. Liu, T. Chen, V. N. Strocov, Y. Song *et al.*, *Nat. Phys.* **18**, 806 (2022).
- [44] A. Kreisel, P. J. Hirschfeld, and B. M. Andersen, *Front. Phys.* **10**, 859424 (2022).
- [45] L. Fanfarillo, *Nat. Phys.* **18**, 738 (2022).
- [46] M. Capone, *Nat. Mater.* **17**, 855 (2018).
- [47] L. Fanfarillo, G. Giovannetti, M. Capone, and E. Bascones, *Phys. Rev. B* **95**, 144511 (2017).
- [48] R. Yu, J.-X. Zhu, and Q. Si, *Phys. Rev. Lett.* **121**, 227003 (2018).
- [49] A. Georges, G. Kotliar, W. Krauth, and M. J. Rozenberg, *Rev. Mod. Phys.* **68**, 13 (1996).
- [50] L. Fanfarillo, A. Valli, and M. Capone, *Phys. Rev. Lett.* **125**, 177001 (2020).
- [51] M. Daghofer, A. Nicholson, A. Moreo, and E. Dagotto, *Phys. Rev. B* **81**, 014511 (2010).
- [52] See Supplemental Material at <http://link.aps.org/supplemental/10.1103/PhysRevB.107.L081114> for details about the model and the DMFT analysis, which includes Refs. [12,13,49–51,54–57].
- [53] M. Capone, L. de' Medici, and A. Georges, *Phys. Rev. B* **76**, 245116 (2007).
- [54] C. Weber, A. Amaricci, M. Capone, and P. B. Littlewood, *Phys. Rev. B* **86**, 115136 (2012).
- [55] A. Amaricci, L. Crippa, A. Scazzola, F. Petocchi, G. Mazza, L. de Medici, and M. Capone, *Comput. Phys. Commun.* **273**, 108261 (2022).
- [56] C. Castellani, C. R. Natoli, and J. Ranninger, *Phys. Rev. B* **18**, 4945 (1978).
- [57] A. Liebsch and H. Ishida, *J. Phys.: Condens. Matter* **24**, 053201 (2012).